Eur. Phys. J. B **41**, 561–568 (2004)
DOI: 10.1140/epjb/e2004-00349-8

THE EUROPEAN PHYSICAL JOURNAL B

Magnetic field rotation in the screw gallium flow

V. Noskov, S. Denisov, P. Frick, S. Khripchenko, D. Sokoloff, and R. Stepanov[a]

Institute of Continuous Media Mechanics, Korolyov 1, 614061 Perm, Russia

Received 14 May 2004 / Received in final form 27 August 2004
Published online 5 November 2004 –

Abstract. The magnetic field induced by the nonstationary screw flow of gallium in a toroidal channel has been investigated experimentally using a gallium prototype of the sodium apparatus developed in the frame of the experimental dynamo program at the Institute of Continuous Media Mechanics, Perm, Russia. The experimental set-up is a rapidly rotating toroidal channel subjected to abrupt braking. The screw flow is initiated by inertial forces pushing liquid gallium through diverters. The regular structure of the induced magnetic field is generated about 0.1 s after the stop of the channel and persists up to 1 s. The induced field is measured by sensors placed outside the channel. The inductive effects observed are attributed to the mean screw flow. The decay laws of the induced regular magnetic field and turbulent magnetic fluctuations are studied.

PACS. 47.65.+a Magnetohydrodynamics and electrohydrodynamics – 07.55.Dd Generation of magnetic fields

1 Introduction

The dynamo mechanism for self-excitation of magnetic fields is considered to be the most important source of magnetic field formation in astrophysical and planetary systems. After successful experiments made by Riga [1] and Karlsruhe [2] research teams, the dynamo has become an open area for experimental studies. The next step in this direction is to extend the variety of specific features of dynamo activity susceptible to experimental verification. A natural part of these studies is to gain insight into subcritical inductive effects.

The systematic efforts to understand the inductive effects in subcritical regimes of von Kárman flows between two counter-rotating discs in VKG (gallium) [3,4] and VKS (sodium) [5,6] experiments have been undertaken within the framework of the dynamo project developed in France. The one– or two-vortex flow was excited in a cylinder tube to which a magnetic field was applied. Several effects initiated by dynamo action were established. In particular, a twist of magnetic loops known as the Parker effect responsible for a link between the toroidal and poloidal magnetic fields in a solar dynamo was revealed. On the other hand, since von Kárman flows are rather complicated, the inductive effect of the inner screw flow must be isolated from that of the background counter-flow. Investigation of the inductive effect of the isolated vortex in the absence of counter-flows is of particular interest for dynamo studies. In order to gain a better understanding of this effect, we have carried out the experiment described below.

Our experiment is a part of the experimental project on the non-stationary MHD-dynamo problem, which is currently under way at the Institute of Continuous Media Mechanics, Perm, Russia [7,8]. The final goal of the project is to realize the dynamo effect in the non-stationary screw flow.

The physical background of this project is similar to that of the Riga dynamo experiment – they both start from the idea of screw dynamo [9] in a current-conducting channel. The research within the Riga project has focused on a *stationary* screw flow in a *cylindrical* channel, generated by a propeller installed in the upper part of the vertical cylinder. The Perm project studies the *non-stationary* screw flow generation in a rapidly rotating *toroidal* channel. After braking, the inertial forces push liquid sodium through fixed diverters.

The new experimental scheme offers some advantages over the original one. In particular, the tests are performed in a closed channel with a limited mass of sodium, eliminating thus the need for gasket application. The experiment uses a low-power motor because the energy is accumulated during relatively long and slow acceleration. Thus, the experimental scheme enables us to realize a variety of regimes, which are of principal interest in the context of the dynamo problem. The experiments with a water prototype [10,11] showed that a diversity of braking regimes and diverters provides a variety of screw flows.

The gallium experiment being interesting in itself can be considered as an intermediate stage between the water and sodium experiments. Conductivity of gallium is substantially lower than that of sodium and therefore the problem of self-excitation of dynamo in the gallium

[a] e-mail: rodion@icmm.ru

Table 1. Comparison of gallium set-up, water prototype and developed sodium dynamo set-up parameters.

	Water	Ga	Na
R, m	0.154	0.0875	0.4
r_0, m	0.04	0.0225	0.12
Mass of the channel, kg	24.5	15.3	300
Mass of fluid, kg	4.86	5.58	115
Moment of inertia (fluid, kg m^2)	0.15	0.045	20
Moment of inertia (channel)	0.58	0.132	50
Frequency of rotation, r.p.s.	30	50	50
Maximal linear velocity, m/s	29	27	140
Nominal Re	1.2×10^6	1.4×10^6	10^7
Effective Re	5×10^5	5×10^5	4×10^6
Effective Rm	-	1.5	40
Minimal braking time, s	0.18	0.05	0.1
Energy of rotation, J	17.3×10^3	6.6×10^3	10^6
Dissipated power, Wt	8.7×10^4	1.3×10^5	10^7
Temperature, °C	20	20	120

system is a challenge. Our prime interest here is to study the effects of advection on the imposed magnetic field.

The subcritical inductive effects (as well as supercritical ones) have been the subject of extensive theoretical investigation. However, there have been only few relevant experimental studies reported in the literature. The papers are mainly concerned with various engineering problems arising in designing of technical devices. Among these, paper [12] is a noteworthy work on the subject. It is concerned with the investigation of inductive effects for a copper tape moving through a flat electromagnet clearance. The induced transverse magnetic field component is observed at $Rm = 4.95$ and $Rm = 8.61$. The magnetic field under the poles becomes inhomogeneous growing from the inlet to the outlet in the direction of motion. The results are in quantitative agreement with theoretical predictions and, admittedly, are essential for understanding the behavior of the magnetic field. However, this study provides only a rough approximation to the situation of our interest, because it examines the motion of a solid rather than a liquid body, which, in addition, has a rather simple form free of rotation.

2 Experimental set-up and measurements

Some technical characteristics concerning the gallium apparatus in comparison with the design parameters of future sodium apparatus for dynamo experiment and of water prototypes [13] are given in Table 1. The gallium set-up (Fig. 1) contains toroidal channel (1) made of insulator (textolite), in which two diverters (2) can be installed opposite each other. The channel is fastened to a horizontal axle, rotated by electromotor (6). Automobile disc braking system (7) is fixed on the same axle. The brake and the clutch are operated by electro-magnets (8).

The rotation velocity of the channel was mainly 45 r.p.s. (rather than 50 r.p.s), which allowed us to avoid some mechanical resonances as well as to exclude coincidence with electrical current frequency. For comparison, we performed some measurements for rotation velocity at 25 r.p.s. (these cases are specifically indicated below). The

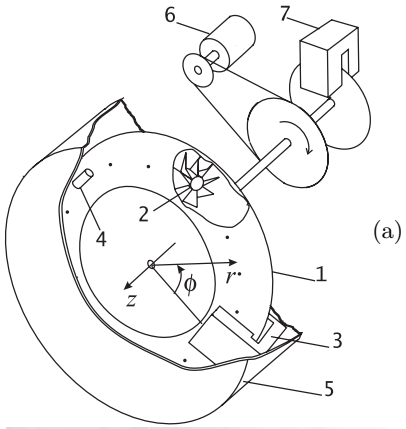

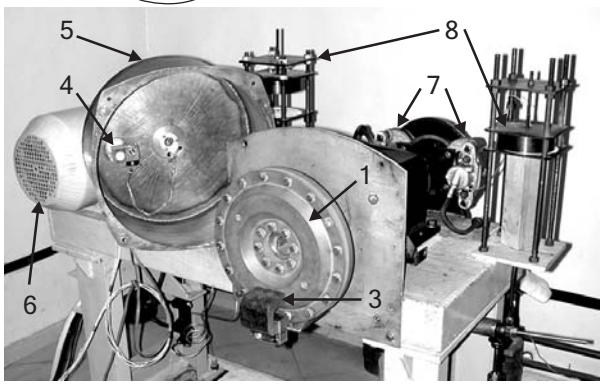

Fig. 1. Experimental set-up (a) scheme of the apparatus (b) photo: 1 – toroidal channel, 2 – diverter with left-hand or right-hand rotation fixed in the channel, 3 – magnet, 4 – magnetic sensor, 5 – steel cover, 6 – electromotor, 7 – brake, 8 – electromagnets. $\phi = 0°$ corresponds to the magnet center. The z-axis is the revolution axis.

rotation velocity and the braking time were kept constant by the electro-mechanical control system. The accuracy of the angular velocity was 0.5 r.p.s. The braking time was 0.077 ± 0.005 s for 45 r.p.s. and 0.043 ± 0.005 s for 25 r.p.s.

The magnetic field was imposed by permanent magnet (3) with the poles 63×20 mm and the spacing between them of 65 mm. The intensity of the magnetic field

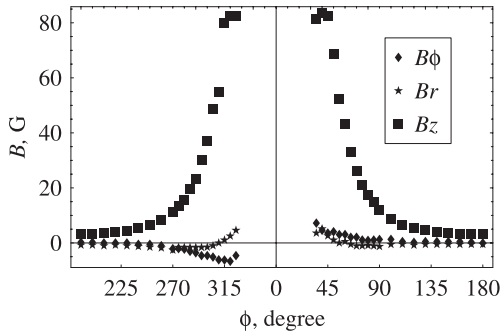

Fig. 2. Distribution of the imposed magnetic field along the central line of the channel versus ϕ: B_ϕ – triangles, B_r – boxes, B_z – stars.

between the poles was about 150 G. The sensor[1] with sensitivity of 0.03 V/G and measuring range of ±80 G was used to measure the intensity of the imposed magnetic field along the center line of the whole channel (Fig. 2). This field was found to be almost perpendicular to the channel axis.

The measurements of the time-variable induced magnetic field were taken using a 3 Axis FluxGate Magnetometer System[2] with sensitivity 4 V/G in the range of ±0.75 G (sensor (4) in Fig. 1). The permanent external magnetic field at the measurement point was compensated. The compensation system allowed measurements of signals at frequency up to 2 KHz. The data acquisition system is based on the Advantec LabCard PCL-1800 with 16 single-ended (or 8 differential) inputs and a 12-bit 330 KHz A/D converter.

Sensor (4) is located at the inner surface of the steel cover (5). Its position is determined in the cylindrical coordinates (r, ϕ, z) as shown in Figure 1, and varied from run to run in the range 55 mm $< r <$ 125 mm and $70° < \phi < 290°$ with the accuracy of 0.5 mm and ±0.5°, respectively. All measurements were done in the plane $z = 46$ mm.

Although we tried to exclude, wherever possible, the ferromagnetic elements and admixture from the space under cover (5), the set-up still contained a few moving solid conductive parts (the driving shaft, draw-bolts, etc.), which involved the imposed magnetic field into their motion. These fields were measured in experiments with an empty channel and then subtracted from the inductive effects arising in the channel with gallium. The magnetic fields, induced by electromotor (6) and electromagnets (8), were weak in the domain of the channel (less as the Earth magnetic field) and decayed before the start of the channel braking.

For a given set of parameters (rotation direction and frequency, magnetic field direction, kinds of diverters, etc.), the magnetic field was determined from a long series of experiments (every experiment gave the magnetic field evolution at one point only). The stability of external and initial conditions was strictly controlled, and the temperature was maintained in the range 22 ± 2 °C. The reproducibility of results was checked in a series of 20 runs. The mean deviation does not exceed 12%. The statistical errors are mainly attributed to the measurement errors, random position of diverters in the channel after braking and turbulent character of the gallium flow.

[1] Produced by Sentron, Model 1SA-1M.

[2] Produced by Applied Physics System, Model 533.

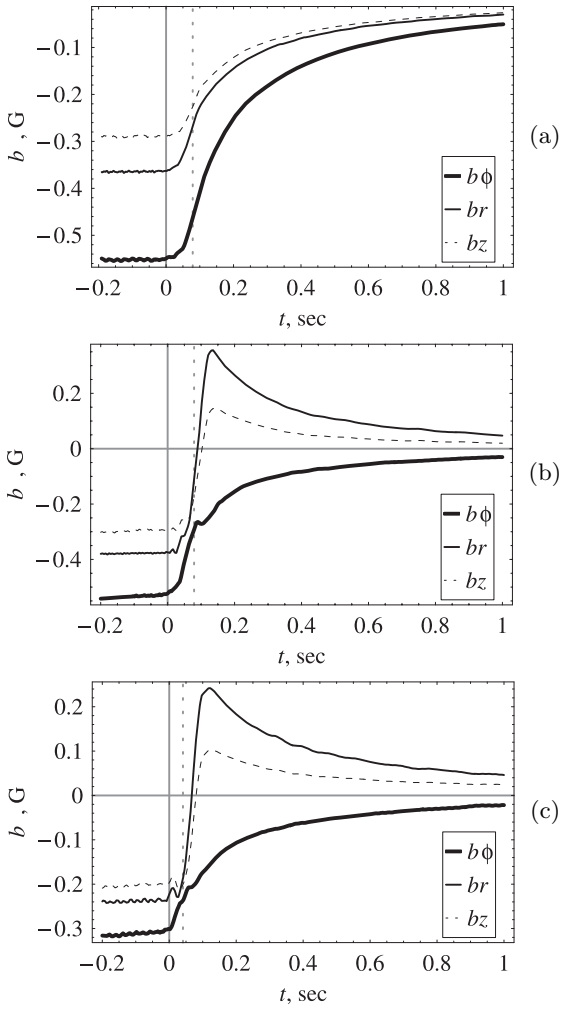

Fig. 3. Measurements of the induced magnetic field components b_ϕ (solid line), b_r (dashed line) and b_z (dotted) at $r = 95$ mm, $\phi = 90°$: (a) the channel without diverters, (b) the channel with two right diverters, (c) the same as (b) at rotation velocity of 25 r.p.s. The time $t = 0$ s corresponds to the start of braking. The end of braking is shown by vertical dotted line.

3 Results

We have investigated the flow in a braking model with and without diverters. In each experiment, three magnetic field components were measured by the sensor located in a fixed position. The magnetic field measurements were started before braking and continued until the motion in the channel stopped. The zero level of sensors was calibrated using the field strength measured at the moment when all transient processes decayed after braking, in practice at $t = 5$ s. Figure 3 shows the evolution of the magnetic field at the point $\phi = 90°$ and $r = 95$ mm.

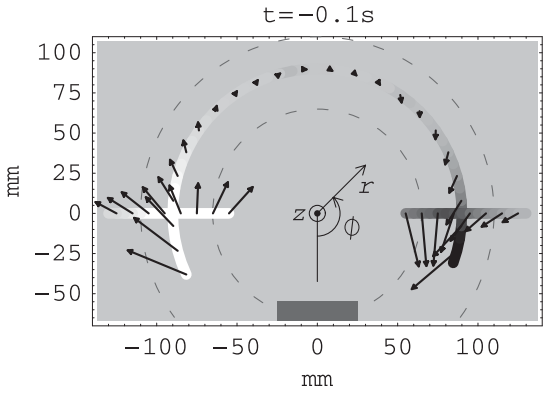

Fig. 4. Induced magnetic field in the plane $z = 46$ mm before braking. The toroidal channel geometry is indicated by dashed lines. The arrows extending from the place of sensor location show the magnetic field projection onto the rotation plane. The gray level of the strip, which passes through the arrow base, defines the value of the z-component of the magnetic field (the maximal b_z is shown by white, the minimal – by black, the background gray corresponds to $b_z = 0$). The magnet is shown by a box at the bottom.

for the channel without diverters (Fig. 3a) and for the channel with diverters (Figs. 3b, c). It is seen that the magnetic fields before braking are identical in both cases. After braking, all components of the magnetic field in the channel without diverters, i.e. in a non-screw flow, decay monotonously. The diverters drastically affect the evolution of r and z magnetic field components. In the example shown in Figure 3, the sign of these components changes at the end of braking. This change of the sign is found to be the most pronounced impact of the diverters on the inductive effect.

The curves in Figure 3c show the evolution of the magnetic field components at the same point as in Figure 3b, but at rotation velocity of 25 r.p.s. It is seen that the induced magnetic field at the rotation velocity of 25 r.p.s. is about two times weaker than that at velocity of 45 r.p.s. This seems to be reasonable because the induced magnetic field is expected to be proportional to velocity and its gradients.

A number of experiments with identical mechanical conditions and different sensor locations was performed to obtain the spatial structure of the induced magnetic field. The diverter position at the instant of braking cannot be prescribed, but it can be defined *post factum*. Some experiments were carried out under identical mechanical conditions and sensor locations to show that the magnetic field evolution after braking is almost independent of the exact diverter position at the instant of braking. A weak dependence was observed in a short interval between the beginning of braking and the establishment of the developed screw flow (see below Sect. 3.2).

Thus from Figure 3 it follows that the behavior of the magnetic field before braking is quite different from that after braking. Below, we analyze the inductive effects of each stage of the magnetic and velocity field evolution.

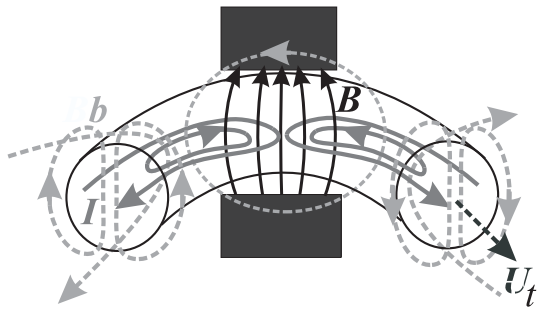

Fig. 5. Scheme of inductive effects in gallium under solid-body rotation: imposed magnetic field $\mathbf{B}$ (black solid arrows), velocity $\mathbf{U}$ of general rotation (black dashed arrow), the loops of induced electrical current $\mathbf{I}$ (gray solid field lines) and induced magnetic field $\mathbf{b}$ (gray dashed field lines). The magnet poles are shown by black boxes.

3.1 Magnetic field advection before braking

Before braking, the motion of gallium in the channel is assumed to be a solid-body rotation. Figure 4 shows the distribution of the *induced* magnetic field measured at $t = -0.1$ s (0.1 s before the beginning of braking, which happened at $t = 0$ s).

For the sake of interpretation simplicity all vectors are decomposed in toroidal and poloidal components. Then the induced magnetic field $\mathbf{b} = \mathbf{b}_t + \mathbf{b}_p$ in a screw flow $\mathbf{U}(r, \phi) = \mathbf{U}_t + \mathbf{U}_p$ with imposed magnetic field $\mathbf{B}$ (mainly assumed poloidal $\mathbf{B}_p$) is governed by the induction equation

$$\partial_t \mathbf{b}_t - (\boldsymbol{\nabla} \times (\mathbf{U} \times \mathbf{b}))_t - \mathrm{Rm}^{-1} \boldsymbol{\nabla}^2 \mathbf{b}_t = \boldsymbol{\nabla}_p \times (\mathbf{U}_t \times \mathbf{B}_p), \quad (1)$$

$$\partial_t \mathbf{b}_p - (\boldsymbol{\nabla} \times (\mathbf{U} \times \mathbf{b}))_p - \mathrm{Rm}^{-1} \boldsymbol{\nabla}^2 \mathbf{b}_p = \boldsymbol{\nabla}_p \times (\mathbf{U}_p \times \mathbf{B}_p) + \mathbf{U}_t \cdot \boldsymbol{\nabla}_t \mathbf{B}_p. \quad (2)$$

Note that the imposed field consists of a strong field B_z between the magnet poles and a relatively weak leakage field around the magnet. This leakage field has a negative gradient along the channel downstream of the magnet and a positive gradient upstream of the magnet (Fig. 2).

The simplest effect is attributed to the transverse magnetic field advection (the second source term in equation (2) $(\mathbf{U}_t \cdot \nabla_t \mathbf{B}_p)_z \equiv U_\phi \partial_\phi B_z$), which produces the positive b_z downstream from the magnet (white strip in the left-hand part of Fig. 4) and the negative b_z upstream from the magnet (black strip in the right-hand part of Fig. 4).

The magnetic field in the plane of measurements is shown in Figure 4 by arrows (the length of each arrow is proportional to $\sqrt{(b_\phi^2 + b_r^2)}$. The main inductive effect is illustrated in Figure 5. The imposed magnetic field B_z is shown by arrows. Because B_z decays with distance from the magnet, the electromotive force $\mathcal{E} = \mathbf{U} \times \mathbf{B}$ also decays. This results in the electrical potential difference,

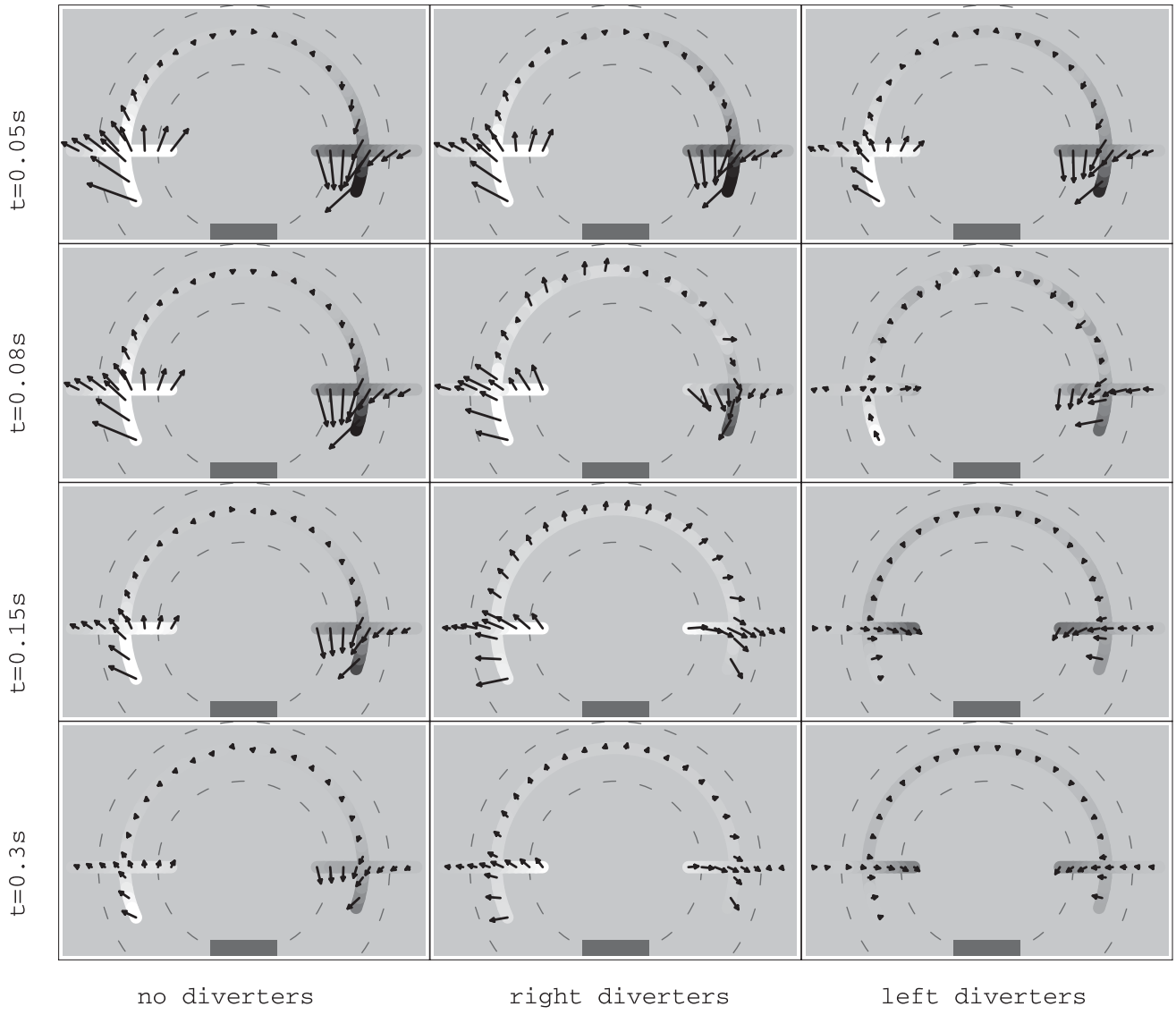

Fig. 6. Magnetic field induced by the flow without diverters (first column), with right (second column) and left (third column) diverters at four moments of time in the plane $z = 46$ mm. The values of time from the top down are 0.05 s (during the break), 0.08 s (end of breaking), 0.15 s and 0.3 s. The magnetic field is represented in the same manner as in Figure 4. A movie with the whole magnetic field evolution can be found at `http://www.icmm.ru/lab4/gallium/movie.avi`.

which gives a loop of electrical current **I** shown by gray solid lines in Figure 5. The current **I** creates the magnetic field **b** in the form of the magnetic dipole directed along the z-axis (Fig. 5). The induced magnetic field is associated with the gradient of the imposed magnetic field and therefore it vanishes in the domain $100° < \phi < 260°$, where the gradient of the imposed magnetic field vanishes (Fig. 2).

3.2 Screw flow formation

Just after the start of braking the flow becomes turbulent and the development of the screw flow takes some time. The screw flow formation begins in the immediate vicinity of diverters and gradually propagates in the channel. From water experiments [7] it is known that the screw flow is established in the whole channel only when the fluid has passed the distance between the diverters in the channel that has already come to a stop. For the braking time $T_b = 0.08$ s and the rotation velocity of about 50 r.p.s., a fully developed screw flow is expected at $t \approx 0.1$ s. Figure 6 shows the results for four moments of time during and after breaking. The magnetic configuration in the second and third panels in the second row of Figure 6 is rather chaotic (in contrast to the case of the flow without diverter – the first column). It happened because the data were obtained from different realizations (in each realization the time evolution of the magnetic field was measured at one point only) and in each of them the diverter position was arbitrary. At $t = 0.15$ s (the third row in Fig. 6), the field distribution is very smooth, which proves the fact that the mean flow becomes homogeneous along the

channel. The latter finding is in agreement with the data of water experiments [7].

3.3 Magnetic field advection in a screw flow

Installation of diverters provides the azimuthal motion $\mathbf{U}_p$ in the channel. The inductive effects induced by this motion are illustrated in Figure 7. The magnetic field configurations for $t = 0.15\,\mathrm{s}$ and $t = 0.3\,\mathrm{s}$ (two last rows in Fig. 6) demonstrate that the magnetic field rotates with the screw flow.

The symmetry properties of inductive effects were studied using the left diverters instead of the right ones (the third column in Fig. 6). b_z becomes positive everywhere at $t = 0.15\,\mathrm{s}$ in the second column (the right diverter) and negative in the third column (the left diverter). The radial component of the magnetic field (b_r in the local coordinate system) also changes its sign, i.e. all arrows are directed to the center of the torus by the right diverter and to the outside by the left one. Note that the inductive effects in the experiments with left diverters are slightly lower than those with right ones. This discrepancy can be explained by some difference in diverter properties (right diverters were made from stainless steel, and left diverters – from caprolon).

In order to verify our interpretation, we extended the study of the symmetry properties of inductive effects. For this purpose, we performed another series of experiments changing the direction of the imposed magnetic field and the direction of rotation (Fig. 8). As expected, the induced magnetic field changes its sign in both cases. If both directions are changed simultaneously, the sign of the induced magnetic field remains the same. Note that this case is equivalent to the magnetic field measurements taken on the opposite side of the channel in the first set of experiments (these measurements are impossible because of the set-up design). The obtained results agree with the dipole symmetry of the induced magnetic field shown in Figures 5, 7. An antisymmetric part relative to the central plane of the torus may occur if the magnetic field is generated by a mean electrical current propagating along the channel. Our measurements did not give any indication that this current exists (it could appear as a result of some turbulent dynamo effect only). The turbulent electromotive force in the presence of rotation, shear and helicity is discussed in [14,15].

4 Discussion

The inductive effects in the nonstationary screw flow of gallium have been measured and investigated. The occurrence of the observed effects can be mainly attributed to the mean flow. Before braking, the induced magnetic field follows the scheme of Figure 5, while the configuration shown in Figure 7 becomes dominant later. However, these schemes do not take into account the toroidal geometry of the channel. Various deviations from the symmetries

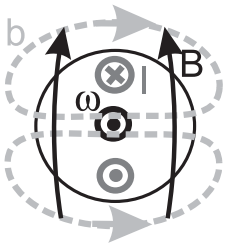

Fig. 7. Scheme of inductive effects caused by azimuthal velocity ω (cross-section of the torus is shown). Here the notation is similar to that used in Figure 5.

expected in the cylindrical flow geometry can be considered as manifestation of some curvature effects. To isolate such effects, one need more detailed measurements and extended theoretical studies.

Some asymmetry of the experiments with the left and right diverters and clockwise and counterclockwise rotation can also be related to turbulent effects. However, these effects appear as minor and their investigation requires special efforts.

After the stop of the channel and rapid rearrangement of the flow, the screw flow and the induced magnetic field decay. The energy of the induced magnetic field ϕ-component in the flow with diverters decreases as $t^{-2.0}$ (black in Fig. 9). The energy of the poloidal magnetic field decreases with the same slope up to $t \approx 0.2\,\mathrm{s}$ and then its decay becomes slower, so that at the later stage this component is stronger than the toroidal one (gray in Fig. 9). The slopes obtained should be compared with the decay laws of kinetic energy of the flow obtained in water experiments [13]. The energy of the rotating motion of water decreases as $t^{-2.1}$, the energy of the motion along the channel – as $t^{-1.7}$ for the flow with and without diverters. Thus, we can conclude that the decay of the magnetic field follows the decay of the velocity field. All slopes are close to the decay law typical for the free-decaying Kolmogorov's turbulence under the assumptions that the maximal scale L is fixed and contains the main bulk of energy E, and the spectral energy flux is constant. Then one obtains $d_t E = E^{3/2} L^{-1}$, i.e. $E \sim t^{-2}$.

It should be noted that at diffusion time t_d ($t_d = r^2/\nu_m \approx 2 \times 10^{-3}\,\mathrm{s}$ for the magnetic diffusivity $\nu_m = 0.2\,\mathrm{m}^2/\mathrm{s}$), the flow advances approximately 0.1 of the channel length provided that the rotation velocity is 50 r.p.s. The decay time of the induced field seems to be weakly dependent on the rotation velocity. It means that the turbulent diffusivity only slightly contributes to the total losses mainly determined by ohmic dissipation.

The analysis of magnetic field fluctuations in the nonstationary fast decaying flow is rather complicated, taking into account that the measurements were made outside the channel. Figure 10 shows the original *non-smoothed* signal at points ($r = 95$, $\phi = 90°$) and its wavelet transform. The wavelet decomposition gives the energy density in the time-frequency plane. The horizontal strip corresponds to 50 Hz noise, the black cone at left is the response of the main generation impulse, which follows the braking.

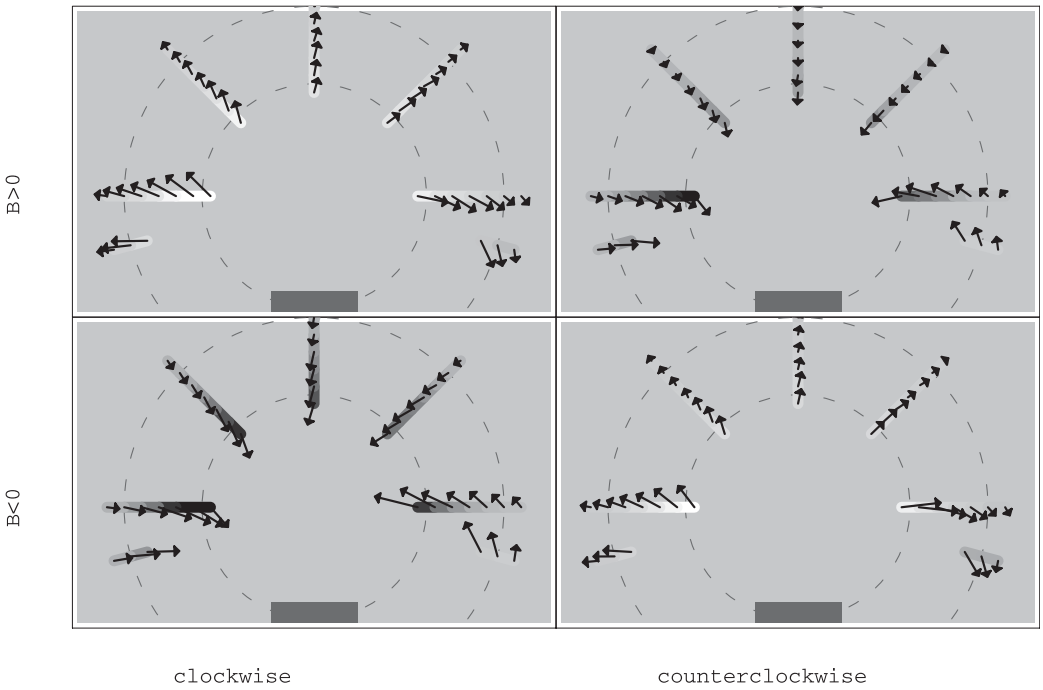

Fig. 8. Symmetry of inductive effects. The first row corresponds to the imposed magnetic field directed as in Figure 4, and the second row – to the imposed magnetic field of opposite direction. The first column presents the results for the clockwise rotation of the torus, and the second column – the results for the counterclockwise rotation. The magnetic field is shown in the same way as in Figure 4.

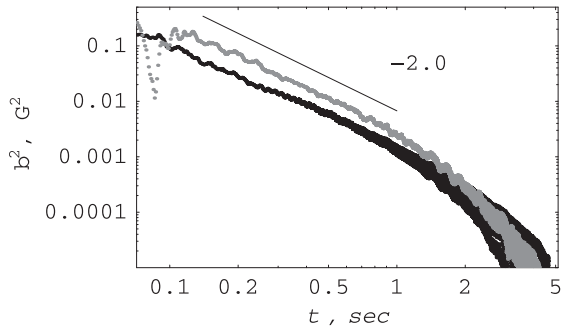

Fig. 9. Decay of the magnetic field energy at the point $r = 95\,\mathrm{mm}$ and $\phi = 90°$: b_ϕ^2 – thick black line, $(b_r^2 + b_z^2))$ – thick gray line, slopes – thin lines.

To describe the energy decay of magnetic fluctuations, we have performed the windowed Fourier transform in the band $10\,\mathrm{Hz} < f < 30\,\mathrm{Hz}$. The total spectral energy in this band decays as $\sim t^{-3.7}$ (Fig. 11). Thus the energy of magnetic field oscillations decays essentially faster than the mean fields (both velocity and magnetic ones). The slope in the power law is the sum of the slopes, characterizing the decay of both mean fields which seems to related with source term $\nabla \times (\mathbf{u}' \times \mathbf{b})$ in the equation for magnetic field fluctuation

$$\partial_t \mathbf{b}' = \boldsymbol{\nabla} \times (\mathbf{u}' \times \mathbf{B}) + \boldsymbol{\nabla} \times (\mathbf{u}' \times \mathbf{b}) + \boldsymbol{\nabla} \times (\mathbf{U} \times \mathbf{b}') + \boldsymbol{\nabla} \times (\mathbf{u}' \times \mathbf{b}')' + \mathrm{Rm}^{-1} \boldsymbol{\nabla}^2 \mathbf{b}', \quad (3)$$

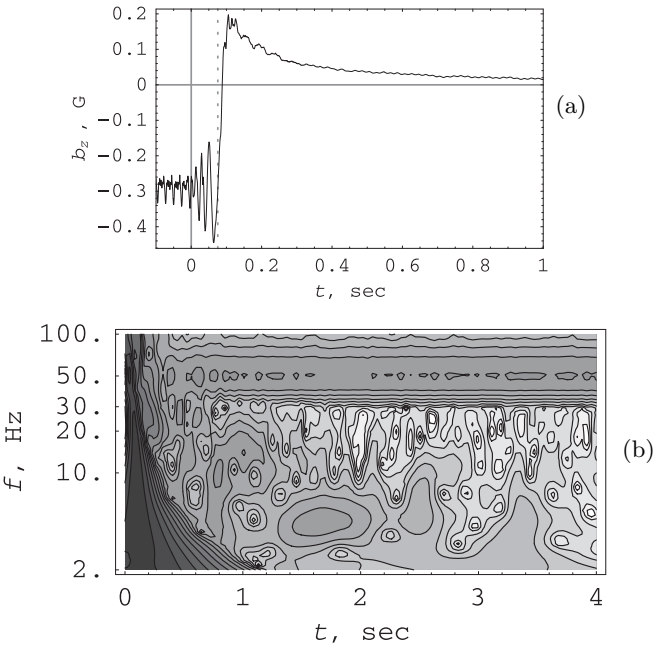

Fig. 10. Magnetic field fluctuations: (a) – non-smoothed signal at a fixed point ($r = 95\,\mathrm{mm}$ and $\phi = 90°$); (b) – its wavelet transform.

where $\mathbf{u}'$ is the pulsation of the velocity field[3].

[3] We are grateful to the anonymous referee for this helpful suggestion.

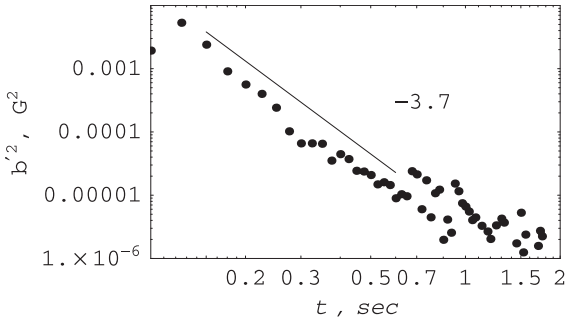

Fig. 11. Decay of the fluctuation energy within the the frequency band from 10 Hz to 30 Hz. Fourier transform is made in the moving window of 0.1 s.

The flow under discussion has the magnetic Reynolds number essentially lower than the critical number for dynamo self-excitation. The advection of the magnetic field is, nevertheless, important, even though consideration is given to the subcritical dynamo regime. The subcritical induction phenomena in astrophysics mainly occur somewhere at the boundary between highly conductive media and weakly conductive (almost nonconductive) media, e.g. vacuum. The channel in our experimental apparatus has the same surrounding. In particular, the magnetic field advection, the magnetic line stretching and other inductive effects are common to the upper layers of the Sun, while the large-scale magnetic field self-excitation due to dynamo action is usually attributed to the lower layers of the solar convective zone. The nonstationary dynamos are quite natural in the astrophysical context, because the life time of some astrophysical flows can be compared with the dynamo time-scale.

It has been found that the regular magnetic field distribution is established very fast, about 0.1 s after the start of braking. This result is of practical importance for future non-stationary sodium experiments aimed at studying the dynamo action, although we have used in this study the insulating shell of the channel whereas the corresponding dynamo experiment requires a conducting channel. To sum up, the impulse experiments open the way to the development of laboratory dynamo experiments with very high magnetic Reynolds numbers.

We thank V.I. Bogdanov for preparation of the experimental set-up. This research was supported by Award #2021 from ISTC.

References

1. A. Gailitis, O. Lielausis, S. Dement'ev, E. Platacis, A. Cifersons, G. Gerbeth, T. Gundrum, F. Stefani, M. Christen, H. Hänel et al., Phys. Rev. Lett. **84**, 4365 (2000)
2. R. Stieglitz, U. Müller, Physics of Fluids **13**, 561 (2001)
3. P. Odier, J.-F. Pinton, S. Fauve, Phys. Rev. E **58**, 7397 (1998)
4. M. Bourgoin, R. Volk, P. Frick, S. Khripchenko, P. Odier, J.-F. Pinton, Magnetohydrodynamics **40**, 3 (2004)
5. M. Bourgoin, L. Marie, F. Petrelis, C. Gasquet, A. Guigon, J. Luciani, M. Moulin, F. Namer, J. Burguete, A. Chiffaudel et al., Physics of Fluids **14**, 3046 (2002)
6. F. Pétrélis, M. Bourgoin, L. Marié, J. Burguete, A. Chiffaudel, F. Daviaud, S. Fauve, P. Odier, J.-F. Pinton, Phys. Rev. Lett. **90**, 174501 (2003)
7. P. Frick, V. Noskov, S. Denisov, S. Khripchenko, D. Sokoloff, R. Stepanov, A. Sukhanovsky, Magnetohydrodynamics **38**, 143 (2002)
8. W. Dobler, P. Frick, R. Stepanov, Phys. Rev. E **67**, 056309 (2003)
9. Y.B. Ponomarenko, Zh. Prikl. Mekh. Tekhn. Fiz. **6**, 775 (1973)
10. S.A. Denisov, V.I. Noskov, D.D. Sokolov, P.G. Frick, S.Y. Khripchenko, Dokl. Akad. Nauk **365**, 478 (1999)
11. P. Frick, V. Noskov, S. Denisov, S. Khripchenko, D. Sokoloff, R. Stepanov, A. Sukhanovsky, in *Proccedings of the IV International Conference PAMIR* (LEGI, Grenoble, 2000), Vol. 1, pp. 183–188
12. I.V. Lavrent'ev, A.Y. Shishko, Magnetohydrodynamics **16**, 288 (1980)
13. S.A. Denisov, V.I. Noskov, A.N. Sukhanovskii, P.G. Frick, Fluid Dynamics **36**, 734 (2001)
14. K.-H. Rädler, N. Kleeorin, I. Rogachevskii, Geophys. Astrophys. Fluid Dyn. **97**, 249 (2003)
15. K.-H. Rädler, R. Stepanov, "*The dynamo in a turbulent screw flow*", *Advances in Turbulence X (Proceedings of the Tenth European Turbulence Conference, Norway, Trondheim, June 29 – July 2, 2004)*, pp. 789–792